Underground Mining Technology 2017 – M Hudyma & Y Potvin (eds)

https://papers.acg.uwa.edu.au/p/1710_18_Collins/

The design, optimisation, and use of the seismic system at the deep and high-stress block cave Deep Mill Level Zone mine

W de Beer *ESG Solutions, Australia*

A Jalbout *Goldcorp, Canada*

E Riyanto *PT Freeport Indonesia, Indonesia*

A Ginting *PT Freeport Indonesia, Indonesia*

M Sullivan *PT Freeport Indonesia, Indonesia*

DS Collins *ESG Solutions, Canada*

Abstract

The PT Freeport Indonesia Grasberg mine in Papua, Indonesia is composed of the Grasberg open pit and four underground mine operations. The Deep Mill Level Zone (DMLZ) is one of the currently active block cave underground operations. The DMLZ orebody presents a number of significant engineering challenges and technical risks when compared to other operating block caves. Due to its mining method and the depth of the operation (+1,500 m), mining-induced seismicity was identified as one of the key factors that will affect the rock mass stability. The seismic system is one of the main tools that is used to track and understand the rock mass response for this cave propagation.

This paper presents initial results from the DMLZ, and includes details about the rock properties, seismic system optimisation using blast data, and seismic analysis examples to help aid in the safety and productivity of the block cave operation.

Keywords: *microseismic, monitoring, block caving, system, optimisation, seismicity*

1 Introduction

PT Freeport Indonesia's (PTFI) Grasberg mine is located in the Sudirman Mountains at an elevation of 3,000 to 4,500 m above sea level (Figure 1). The mine complex produces about 250,000 tonnes per day of material from Grasberg open pit, and four other active underground operations and projects under construction, i.e. Deep Ore Zone (DOZ), Big Gossan (BG), Grasberg Block Cave (GBC) and the Deep Mill Level Zone (DMLZ). The mine complex produces mainly copper and gold.

The DMLZ mine is the fourth lift of caving in the East Ertsberg Skarn System (EESS) and lies 500 m below the currently producing mine (DOZ) and approximately 2,000 m below surface. There is approximately 1,500 m of caved material above the mine (Figure 2). The DMLZ mine represents about a half billion tonnes of ore and there are around 2,450 drawpoints planned, with the scheduled daily tonnage planned to peak at around 80,000 tonnes per day. Grades are 0.87% copper and 0.71 g/t gold. The mine life is projected through to 2041, and at full production the DMLZ will have around 700 active drawpoints in operation at any given time (Casten et al. 2016).

This paper starts with a summary section on the main geology and rock properties of the DMLZ, followed by sections on the seismic system assessment after installation, and seismic analysis examples that are being used to help maintain the safety and productivity of the mine operation.

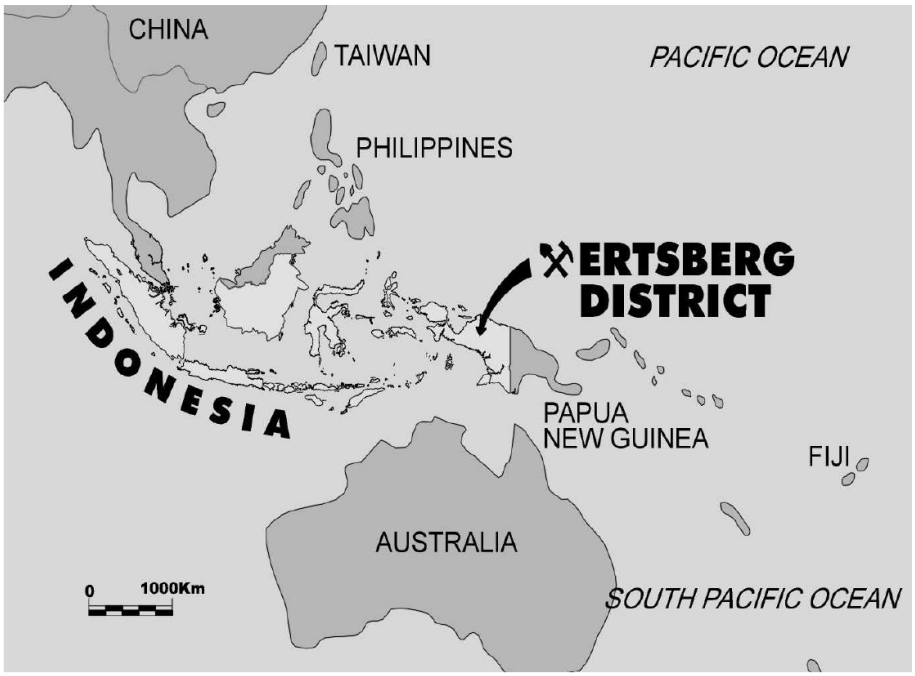

Figure 1 Location of PT Freeport Indonesia operations (Kurniawan et al. 2016)

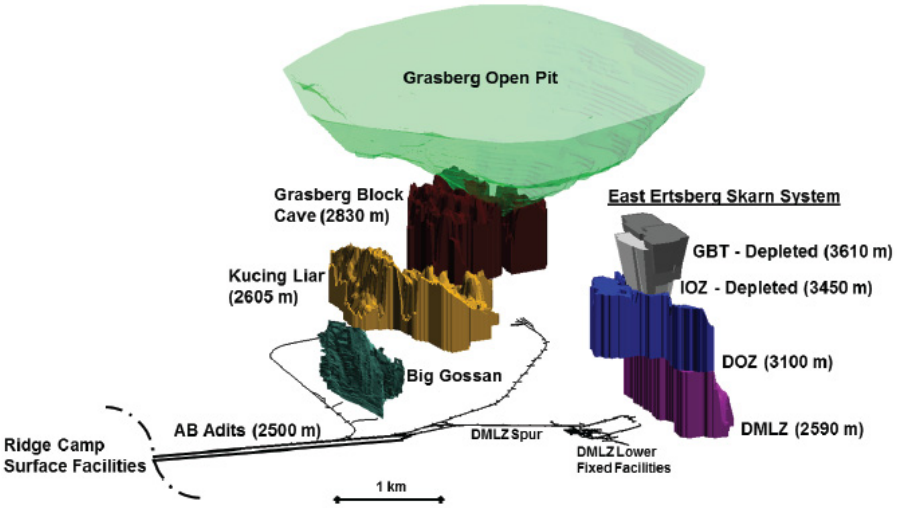

Figure 2 Freeport Indonesia orebodies and primary AB Adit (Ali Budiardjo Adit for access tunnel to DMLZ, GBC and Big Gossan) access (Casten et al. 2016)

2 Geology

The geology of the DMLZ extraction level is illustrated in Figure 3. Principal geological units are the Ertsberg diorite, Waripi and Kembelagan limestones, and skarns located at the diorite contact. Major structures include several splays of the northwest trending faults.

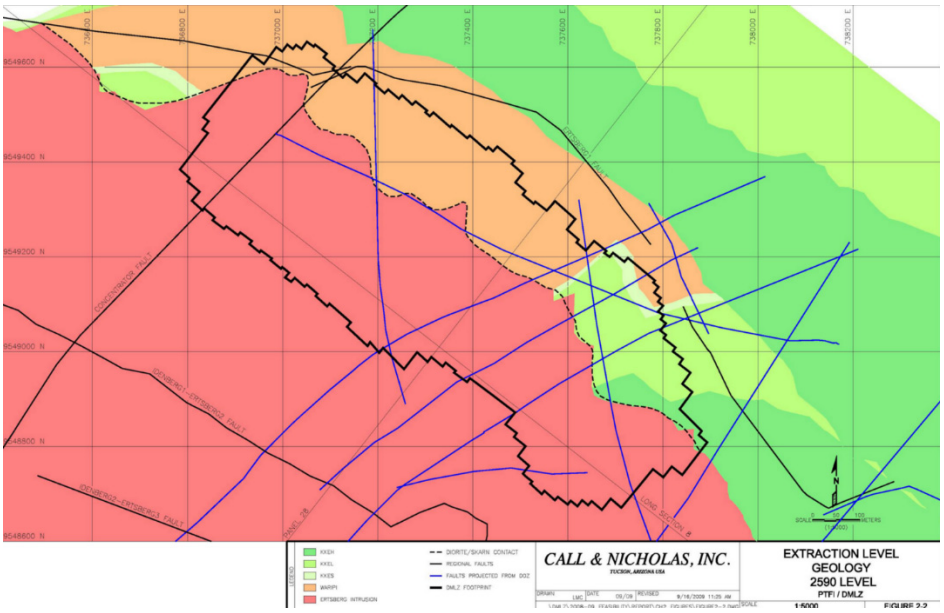

Figure 3 The geology of the extraction level (Call & Nicholas, Inc. 2009)

2.1 Major structure and rock mass characterisation

Figure 4 illustrates the geology along DMLZ panel drift 28. In addition to the steeply dipping Idenberg and Ertsberg Faults, the Yellow Valley Syncline is illustrated to the north of the GBC, IOZ, DOZ, and DMLZ. Skarns are the predominant unit in contact with the Ertsberg diorite. The rock mass strengths used in this study are summarised in Tables 1 and 2 (Call & Nicholas, Inc. 2009).

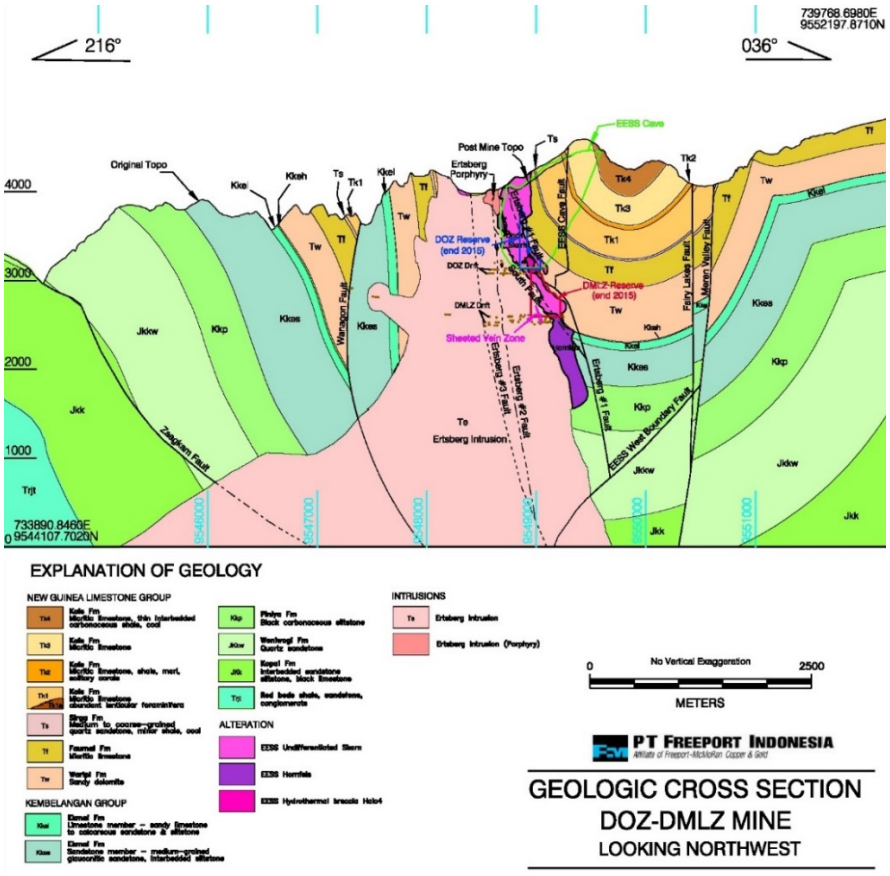

Figure 4 Geology cross-section in DMLZ mine – section looking northwest (P. Warren, pers. comm., June 2017)

Table 1 Intact material properties summary

Rock type	Uniaxial compressive strength (UCS)		Tensile strength		Density			
	Average (MPa)	Standard deviation (MPa)	Average (MPa)	Standard deviation (MPa)	Average (kg/m^3)	Standard deviation (kg/m^3)	E (GPa)	v
Limestone	141	59	9.9	3.3	2,850	145	64	0.30
Skarn	120	55	11.2	4.2	3,458	662	75	0.30
Diorite	157	39	11.5	2.1	2,704	184	52	0.30

Table 2 Intact cohesion and friction angles for DMLZ rock types

Rock type	Friction angle	Cohesion (MPa)
Limestone	45.6	30.7
Skarn	49.3	8.2
Diorite	48.4	30.9

3 Seismic system array

3.1 Summary

The seismic array comprises of a mixture of uniaxial and triaxial 15-Hz geophones installed in boreholes ranging from short 10 m upholes to longer downholes up to 600 m in length. The sensor spacing is purposely more dense around the expected cave development in order to provide more accuracy and sensitivity in this region. A few of the sensors above the cave zone are sacrificial.

3.2 Seismic array site optimisation

To date, two array optimisations have been performed. In June 2016 a single velocity model (termed here 1DVM) was established using ten drawbell blasts with known locations (Figure 5), and in March 2017 a mesoscale, semi-static velocity model which incorporates gross geology and the cave outline (termed here 3DVM (Collins et al. 2014; Pinnock et al. 2016) was derived using oriented sensors and known geological domains and excavations (Figure 6). Blast locations were determined on mine plans to within 5 m of the centre position of a planned blast volume. The optimal 1DVM in 2016 was found to be V_P = 5,710 m·s^{-1} and V_S = 3,240 m·s^{-1}, where $V_{P/S}$ is the P-wave/S-wave velocity, respectively. Table 3 displays the absolute location trueness of the ten blasts used. Overall, the root mean square (RMS) location trueness (Equation 1) was 26.6 m, with a slight bias to the north. Note that real events in which S-waves can be identified are expected to have improved accuracy.

$$RMS = \sqrt{\frac{\sum_1^n difference^2}{n}} \quad (1)$$

The March 2017 3DVM was built using eleven blasts with clear signals (Figure 7). These were production (DMLZ) or secondary breaking (DOZ) blasts which could be identified with a fair degree of confidence. The results are shown in Table 4.

It is expected that location accuracy will decrease as the cave zone develops in size (some sensors will be lost) and the rock mass becomes more attenuating. Installation of additional uniaxial geophone sensors are planned in specific regions around the cave to help improve location accuracy over time. The 3DVM will be regularly updated as the cave zone develops upwards and outwards.

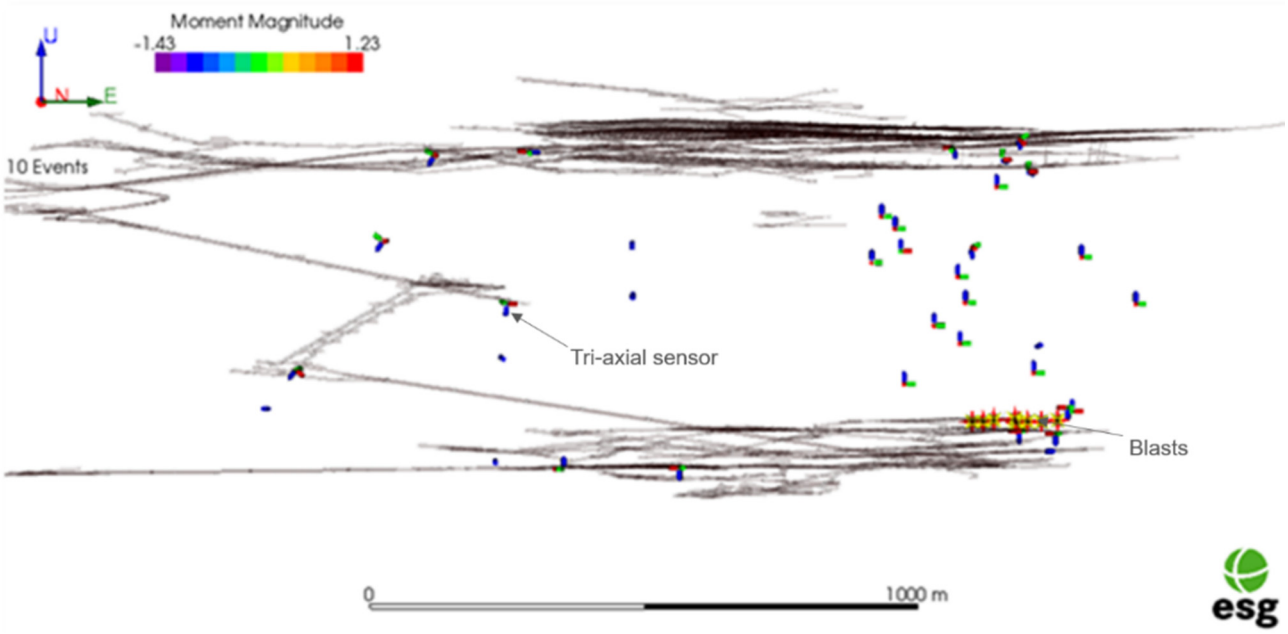

Figure 5 Location of the working sensors and ten blasts used for site optimisation in June 2016. The blasts are all near to the initial cave development providing a good estimate of the absolute location accuracy in this area

Table 3 Quantification of the location trueness using blast data at the site (2016)

		Known coordinates (m)			Calculated coordinates (m)			Difference (known – calculated) (m)			
Date	**Time**	**North**	**East**	**Elevation**	**North**	**East**	**Elevation**	**North**	**East**	**Elevation**	**Distance**
02 Apr 16	17:16:26	9549201	737622	2612.1	9549186	737617	2609.9	15.3	5.6	2.2	16.4
02 Apr 16	17:16:26	9549162	737554	2608.1	9549145	737558	2619	17	-4.1	-10.9	20.6
04 Apr 16	17:03:07	9549159	737551	2608.1	9549148	737553	2630.3	11	-1.8	-22.2	24.8
04 Apr 16	17:03:07	9549148	737505	2612.3	9549137	737508	2624.1	11.4	-3.8	-11.8	16.8
07 Apr 16	17:47:25	9549164	737592	2609.4	9549142	737611	2630.4	21.6	-18.5	-21	35.4
07 Apr 16	17:58:14	9549147	737485	2609.4	9549130	737472	2603.9	17.3	12.4	5.5	22
07 Apr 16	17:30:14	9549153	737546	2608.1	9549138	737555	2633.5	14.7	-9	-25.4	30.7
08 Apr 16	17:30:15	9549146	737465	2609.4	9549137	737479	2628.9	9.4	-14.2	-19.5	25.9
08 Apr 16	17:53:00	9549155	737567	2609.4	9549121	737546	2598.7	33.5	20.3	10.7	40.6
18 Apr 16	17:29:56	9549149	737543	2613.9	9549139	737543	2634.8	10.3	0.5	-20.9	23.3
							RMS:	**17.5**	**11.2**	**16.7**	**26.6**

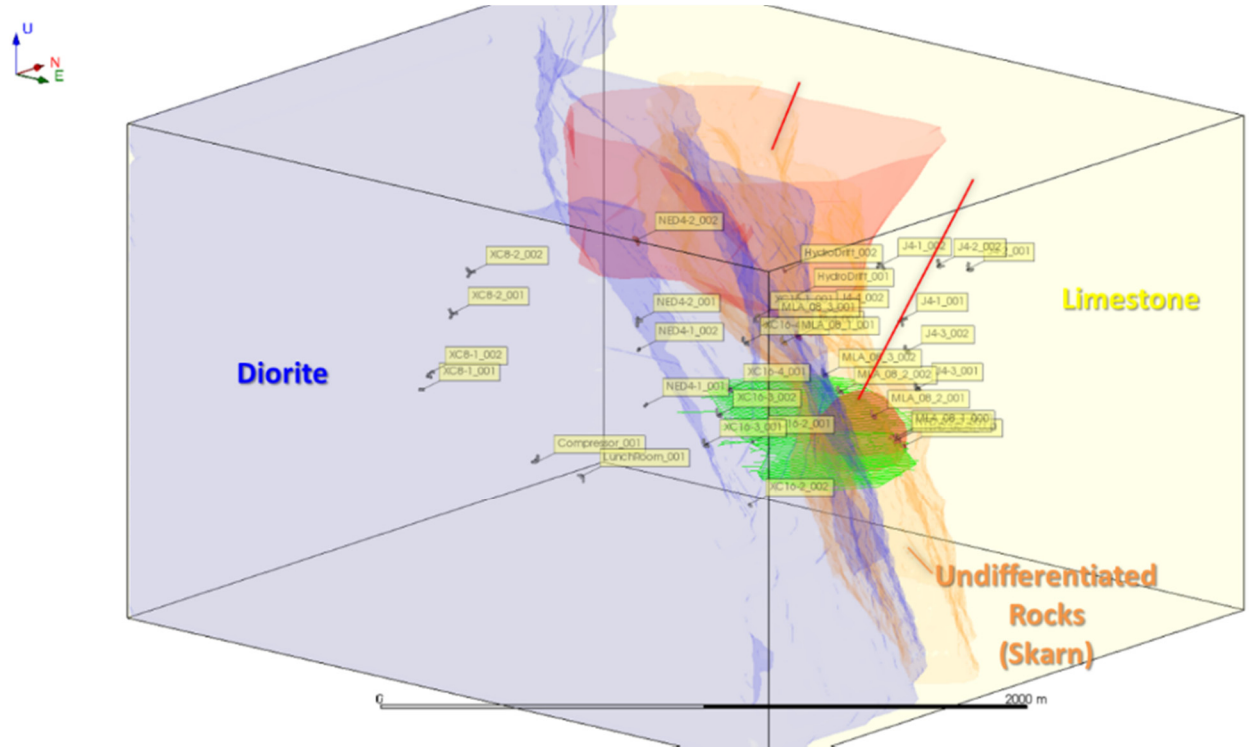

Figure 6 Geological domains and alterations to the rock mass by mining effecting the velocity structure used in the March 2017 3DVM construction

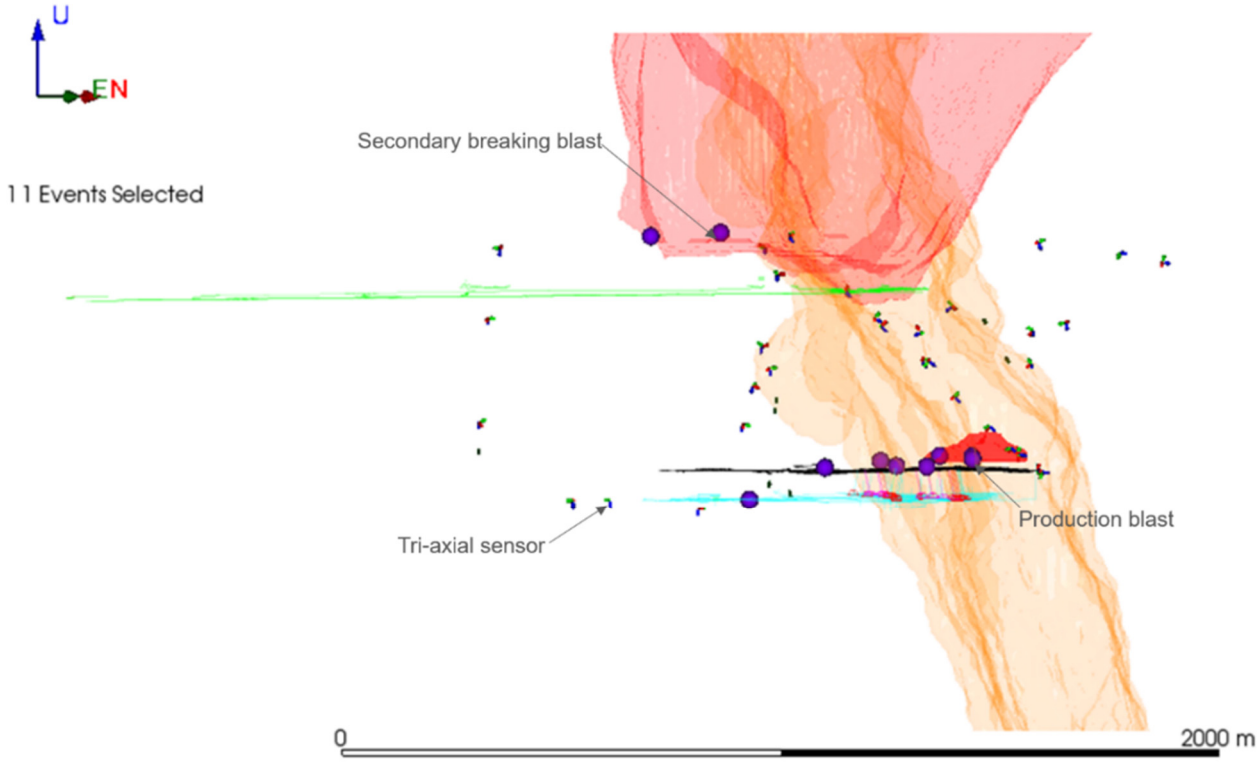

Figure 7 Blasts and sensors used in March 2017 3DVM construction

Table 4 Average seismic velocities in the four identified mesoscale domain at the DMLZ mine

Domain	V_P (m s^{-1})	V_S (m s^{-1})	Comment
Diorite	5,590	3,175	V_P estimated using calibration blasts V_S estimated using calibration blasts
Limestone	4,910	2,840	V_P estimated using calibration blasts V_S estimated assuming Poisson's ratio = 0.25
Undifferentiated rocks (skarn)	6,225	3,450	V_P estimated using calibration blasts V_S estimated using calibration blasts
Caves (filled)	3,110	1,725	V_P estimated to be 50% of skarn vel V_S estimated to be 50% of skarn vel

4 Rock mass seismic response

4.1 Introduction

The DMLZ is a seismically active mining area. The microseismic monitoring system can detect events down to moment magnitude M_W = -2.1, while there is a substantial population of events larger than M_W = 0.0 (Figure 8). Note that, since the dataset represented in Figure 8 was acquired, an event of M_W = 2.25 has occurred. The seismic system at the DMLZ currently consists of 15-Hz geophone sensors. A few lower frequency 4.5-Hz geophones are planned to be installed in the near future to help improve the accuracy of seismic source parameters of larger magnitude events. The DMLZ mine staff are developing a plan to manage the hazard associated with mining in high-stress ground. The analysis is in early stages, and starts with the spatial distribution of seismicity, followed by relating events magnitudes and distances from damage. Different seismic source parameters are being analysed (seismic moment, seismic energy and apparent volume). This section focuses on three aspects: zonation, significant events, and ground motion.

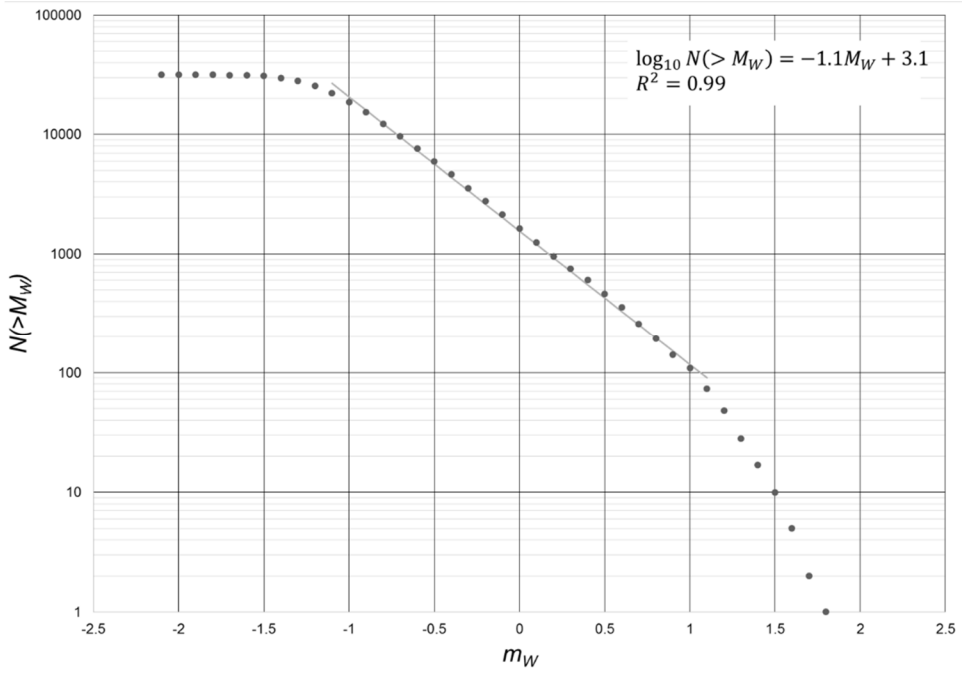

Figure 8 Complimentary cumulative magnitude frequency plot for events in the DMLZ, March 2016 to early October 2016

4.2 Zonation

Periodic snapshots of seismicity (Figure 9) reveal a halo of seismic activity propagating in advance of the undercut face. This halo is variously termed the 'zone of influence of the cave', the 'cave zone', or the 'seismogenic zone'. Unfortunately, this is also the area where people work, requiring a management tool to aid in deciding when and where work can take place. The area is characterised in space and time by dividing it into zones. Zones are characterised by the amount of seismicity, degree of damage (as a proxy for susceptibility to damage – see Figure 10), times of increased hazard (Figure 11), and distance from seismicity (Figure 12). The footprint around and below the current cave may then be divided into different zones (Figure 13), where a 'red zone' would be a no-go zone during a particular exclusion period.

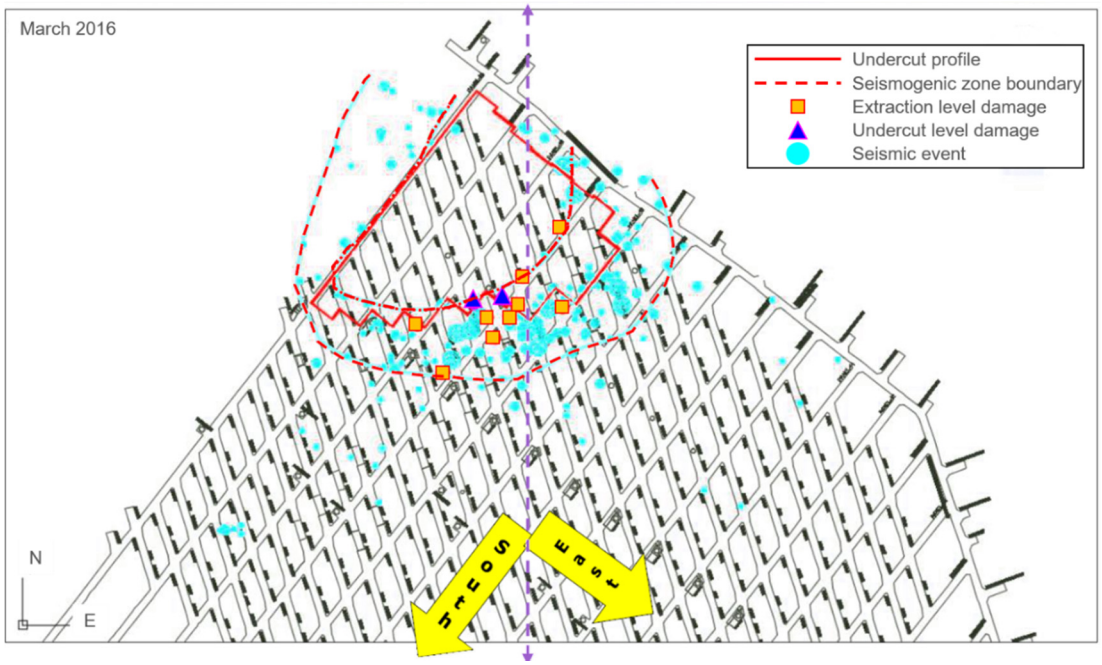

Figure 9 Plan view of seismicity around the extraction level, DMLZ in March 2016. Note the halo of activity in advance of the undercut, and the clustered distribution of damage

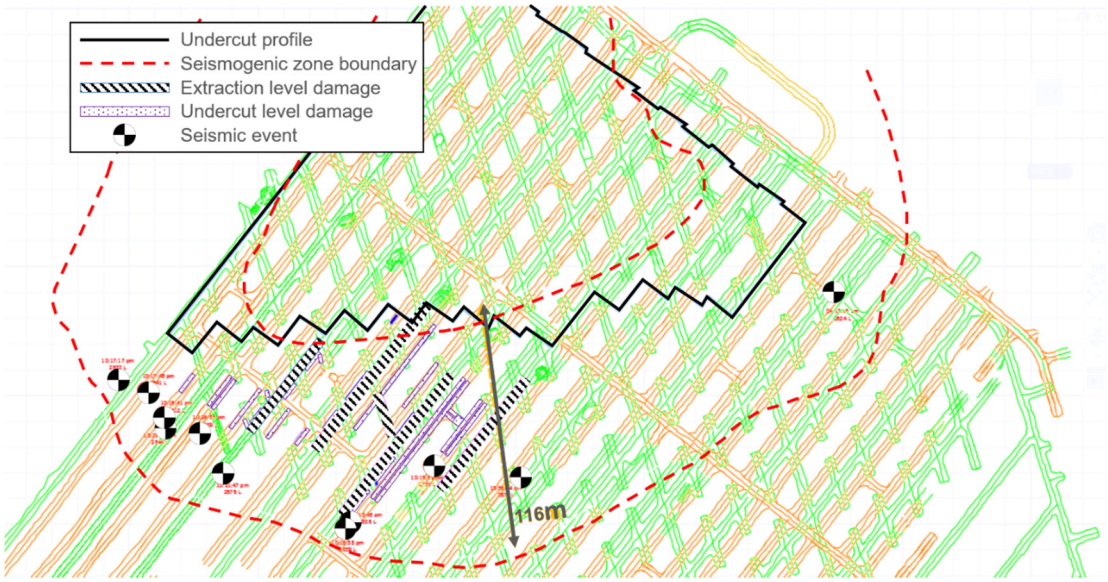

Figure 10 Damage mapping and plan view of seismicity around the extraction level, DMLZ. The 'beach ball' symbols are not intended to depict source mechanisms

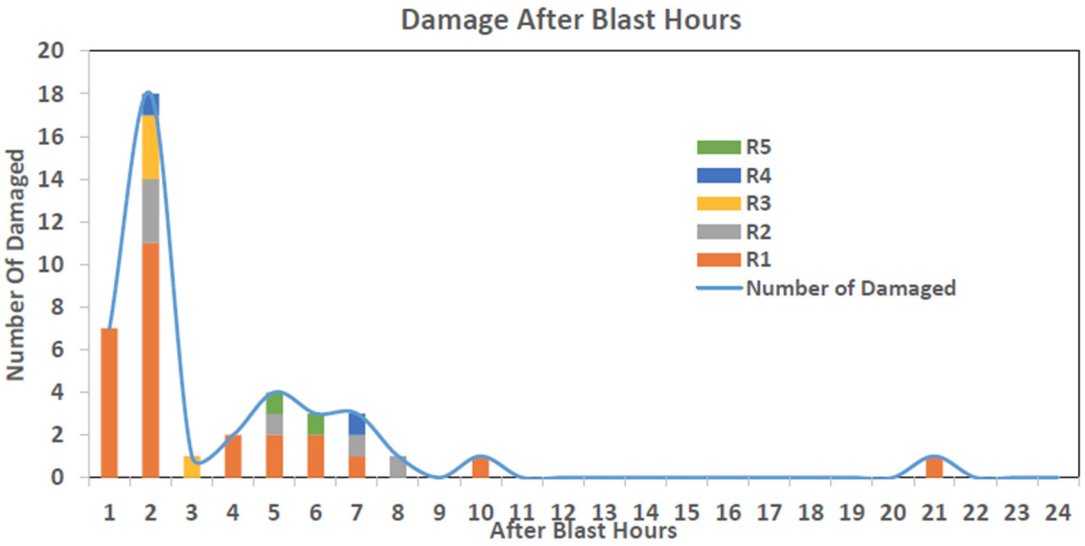

Damage Scale	Rock Mass Damage	Rock Support Damage	Typical Event	Depth of Damage
R1	No damage, minor loose	No damage	Onset of Bulking	0
R2	Minor damage, less than 1t displaced	Support system loaded, loose in mesh, plated deformed	Bulking	<0.25m
R3	1-10t displaced (<10m^2 area of damage)	Some broken support	Shakedown or Strainburst	0.25-0.75m
R4	10-100t displaced (<50m^2 area of damage)	Major damage to support system	Strainburst	0.75-1.5m
R5	100+ t displaced (>50m^2 area of damage)	Complete failure of support system	Rockburst	>1.5m

Figure 11 Statistics of time after microseismic events and damage. Number of damage locations is plotted against time after blasts

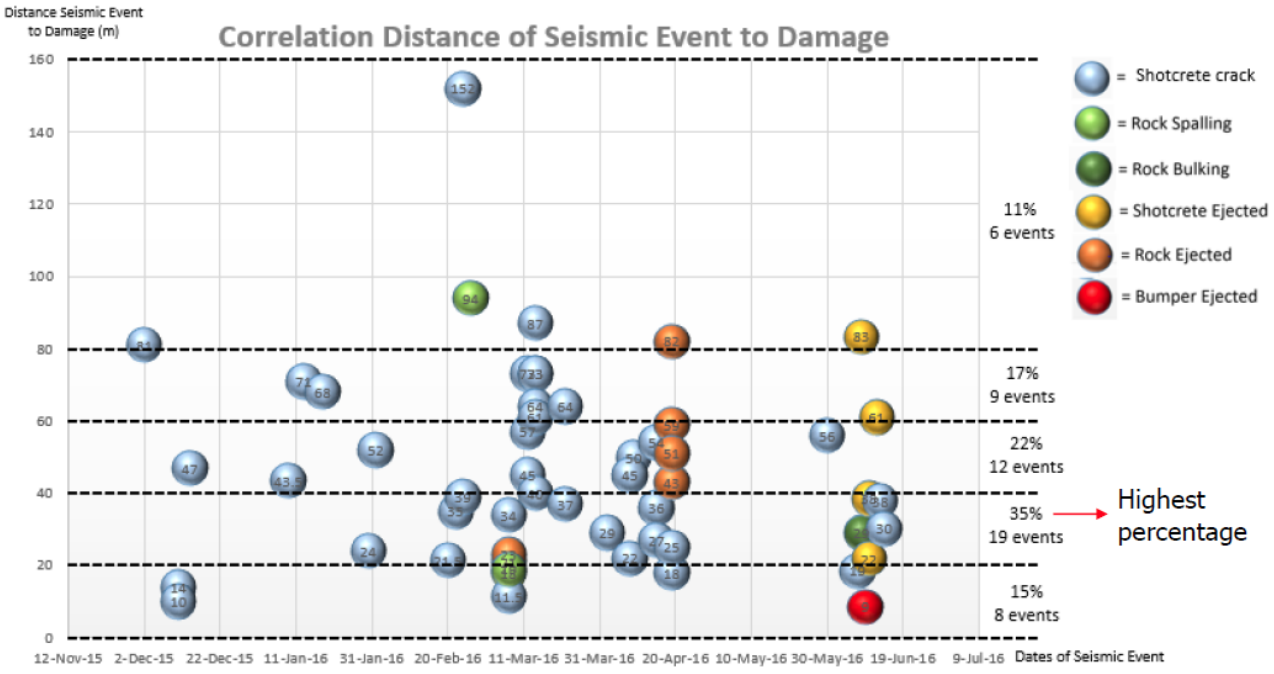

Figure 12 Correlation between distance from seismic events and damage

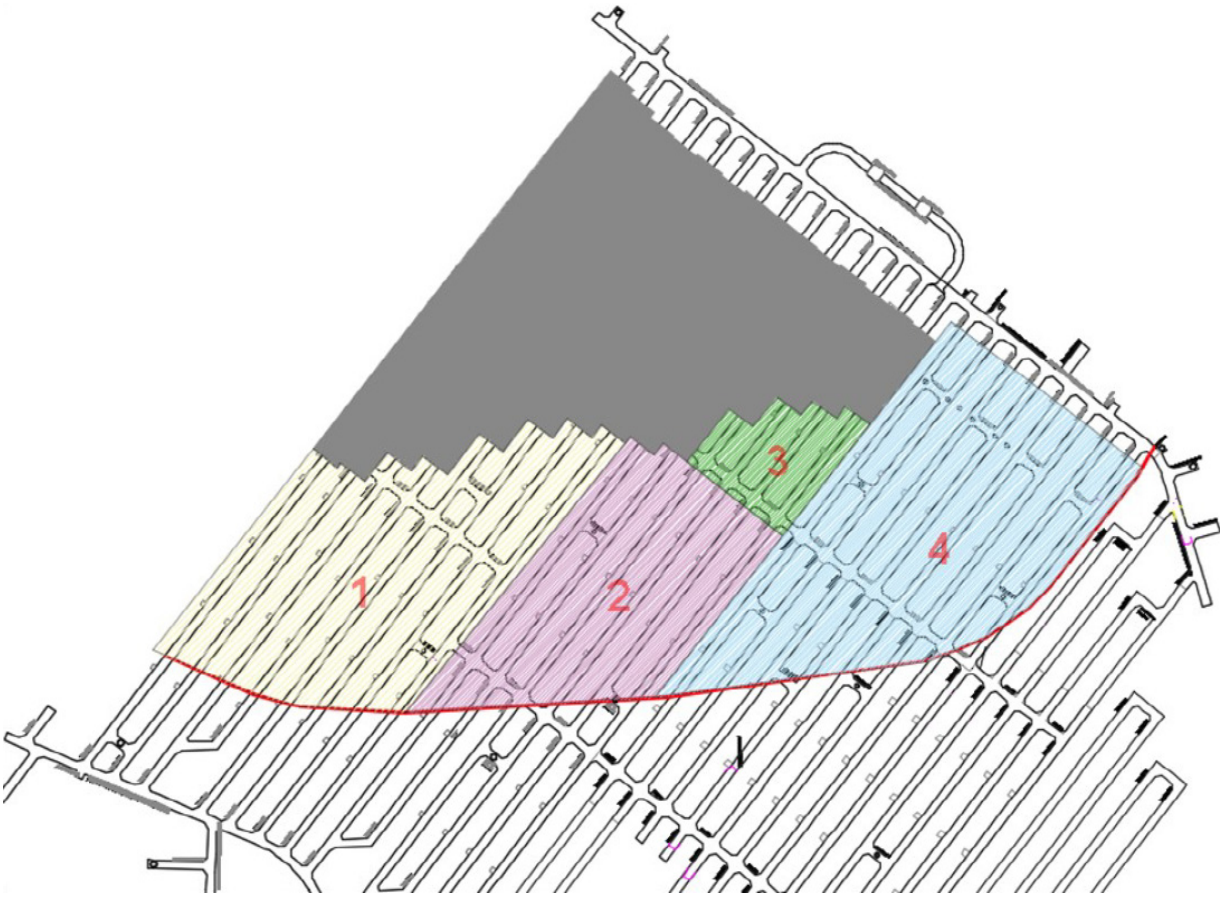

Figure 13 Near-cave seismic zones. The colours range in warmth from 'no-go' (red) to 'safe' (green). Numbers are simply identifiers from left to right (or west to east)

4.3 Peak particle velocity scaling relationships

Figure 14 presents a peak particle velocity (PPV)–distance–magnitude analysis of events which occurred in the DMLZ from March to October 2016. As expected, a generally increasing trend with magnitude is observed. The empirical formula is useful for determining expected PPV at different regions around the mine, especially at important infrastructure tunnels and access haulage ways. A 95% confidence fit is made to provide more conservative estimates of the PPV (Kaiser et al. 1996).

$$\log(PPV) = 1.01 \times M_W - 1.02 - 1 \times \log(R) \quad (2)$$

where *PPV* is the peak particle velocity at a distance *R* from an event of moment magnitude M_W.

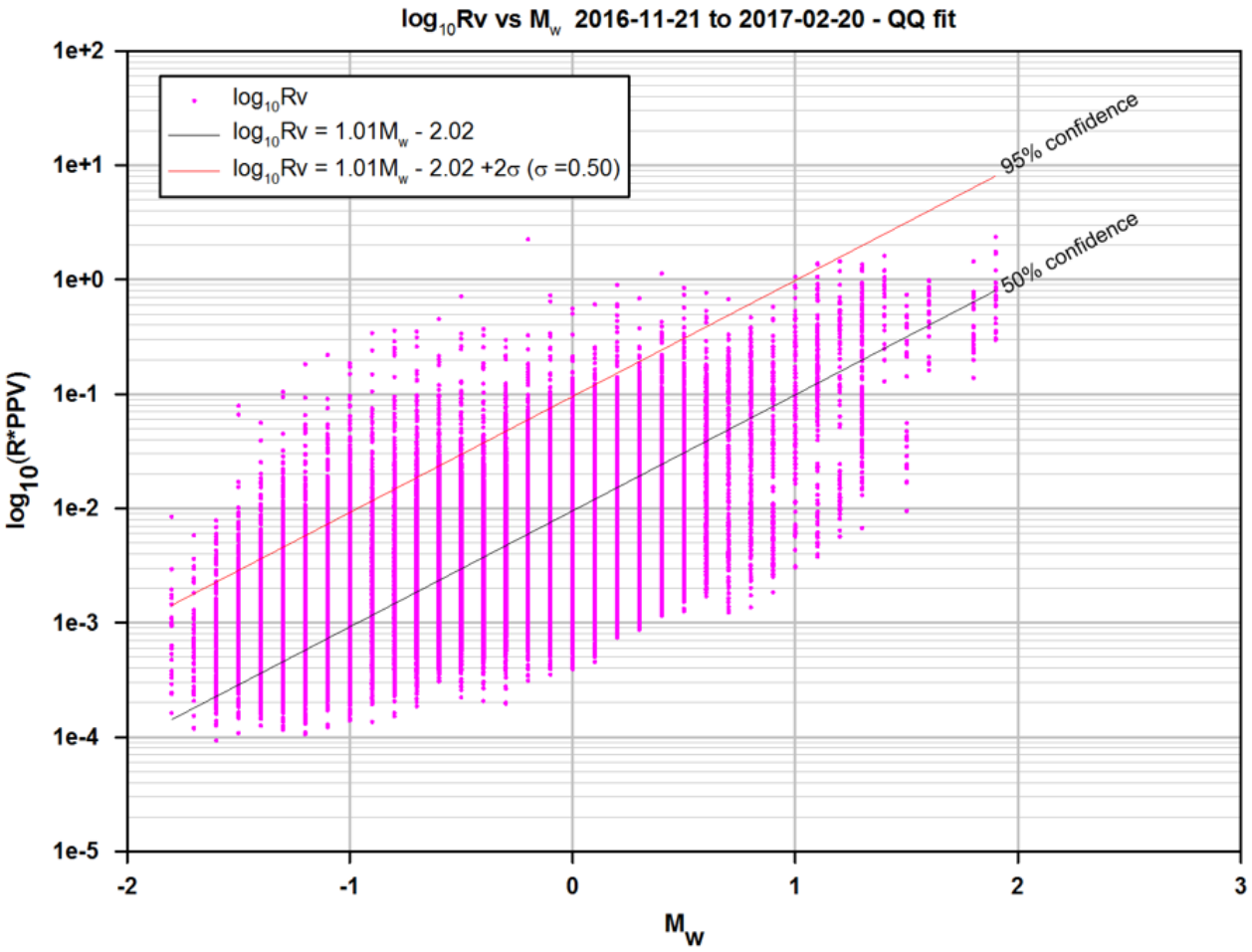

Figure 14 The PPV design scaling relation determined for the site. This relation can be used to estimate the peak particle velocity (peak ground velocity) around tunnel perimeters and throughout the rock mass, and can also be used in seismic hazard calculations

5 Conclusions

A key focus of the data analysis at the DMLZ to date has been to work towards the development of re-entry and exclusion protocols. A comprehensive descriptive record has been assembled of the evolution of the seismogenic zone (Figure 15) on a monthly basis. By combining this evolution with the zonation and damage mapping, hazard zones have been demarcated. When a seismic event exceeds a threshold (e.g., M_W = -0.3) or the rate of seismicity exceeds a certain limit (e.g., three threshold events per hour), the seismic hazard is considered as high. A protocol takes effect and the work force may be evacuated (or excluded) from a 'red zone' (Figure 16).

In the process of establishing data gathering and analysis procedures, the foundations have been laid for interpreting the physics of the rock mass response. The aim of this would be to understand the rock mass response to mining by understanding the evolution of stress in the rock and to manage it by optimising the support and blasting design.

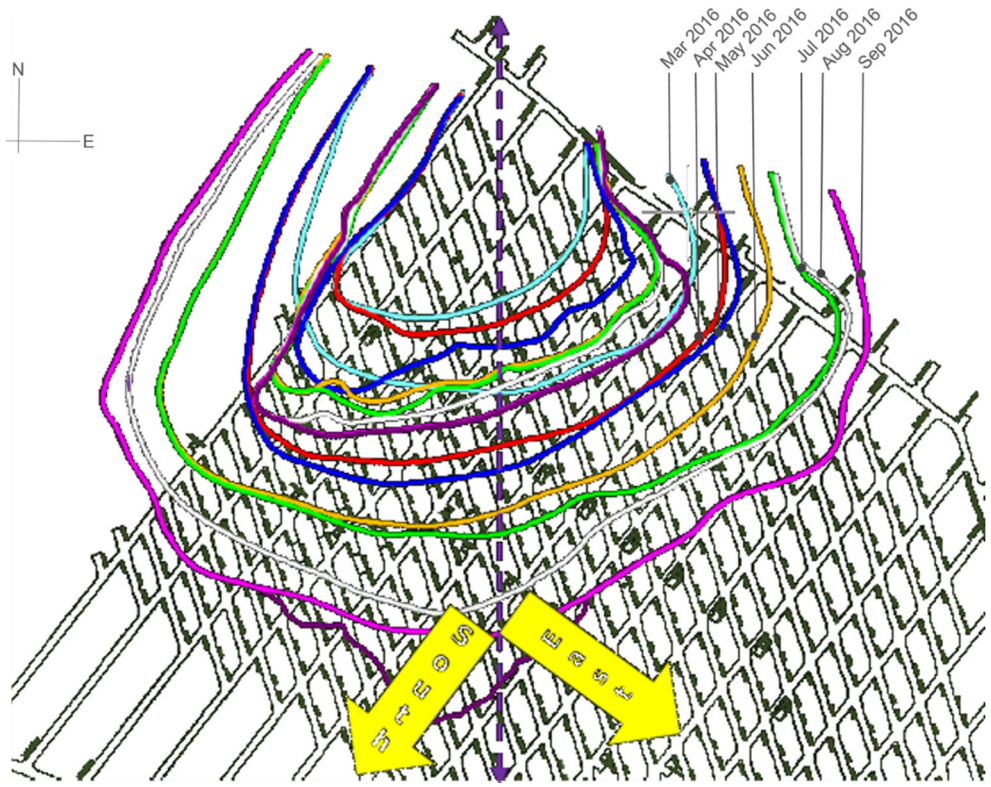

Figure 15 Summary of a timelapse sequence of the seismogenic zone development

Figure 16 Indication underground at DMLZ of the different zones based on seismic hazard

Acknowledgement

The authors appreciate the authorisation from the senior management of PT Freeport Indonesia to publish this paper.

References

Call & Nicholas, Inc. 2009, *Geomechanical Feasibility Study for DMLZ*, report by Call & Nicholas, Inc., Tucson.

Casten, T, Parinta, A & Rumbino, H 2016, 'Deep Mill Level Zone – from feasibility to production', *Proceedings of the Seventh International Conference & Exhibition on Mass Mining*, The Australasian Institute of Mining and Metallurgy, Melbourne, pp. 681–688.

Collins, DS, Toya, Y, Pinnock, I, Shumila, V & Hosseini, Z 2014, '3D velocity model with complex geology and voids for microseismic location and mechanism', in M Hudyma & Y Potvin (eds), *Proceedings of the Seventh International Conference on Deep and High Stress Mining*, Australian Centre for Geomechanics, Perth, pp. 681–688.

Kaiser, PK, McCreath, DR & Tannant, DD 1996, *Canadian Rockburst Support Handbook*, Geomechanics Research Centre, Laurentian University, Sudbury.

Kurniawan, A, Sjadat, A & Akhasyah, M 2016, 'Rehabilitation of the collapsed panel 1K north in the deep ore zone block cave mine', *Proceedings of the Seventh International Conference & Exhibition on Mass Mining*, The Australasian Institute of Mining and Metallurgy, Melbourne, pp. 763–768.

Pinnock, I, Collins, DS, Toya, Y, Shumila, V & Hosseini, Z 2016, 'Large event sequence analysis and 3D velocity models for seismic event location accuracy', *Proceedings of the Seventh International Conference & Exhibition on Mass Mining*, The Australasian Institute of Mining and Metallurgy, Melbourne, pp. 879–884.